Disconnections at translation domain boundaries in epitaxial GaN

2002 J. Phys.: Condens. Matter 14 12709

(http://iopscience.iop.org/0953-8984/14/48/307)

INSTITUTE OF PHYSICS PUBLISHING JOURNAL OF PHYSICS: CONDENSED MATTER

J. Phys.: Condens. Matter **14** (2002) 12709–12715 PII: S0953-8984(02)54137-0

Disconnections at translation domain boundaries in epitaxial GaN

G P Dimitrakopulos[1], Th Kehagias[1], Ph Komninou[1,3], G Nouet[2] and Th Karakostas[1]

[1] Department of Physics, Aristotle University of Thessaloniki, 54124, Thessaloniki, Greece
[2] ESCTM-CRISMAT, UMR 6508 CNRS, ISMRA, 6 Boul. Marechal Juin, 14050 Caen Cedex, France

E-mail: komnhnoy@auth.gr

Received 1 October 2002
Published 22 November 2002
Online at stacks.iop.org/JPhysCM/14/12709

Abstract

Translation domain boundaries on $\{1\bar{2}10\}$ planes are observed in MBE-grown epitaxial GaN on (0001) sapphire, by transmission electron microscopy. Structural models are distinguished using experimental and simulated images. The boundaries exhibit disconnections that may accommodate transformations between distinct structural models. A topological method is utilized to obtain an account of such disconnections *a priori*. The experimentally observed cases are characterized on the basis of this account.

1. Introduction

Defects in semiconductors may degrade material properties, and extensive efforts have been undertaken to elucidate their role and to reduce their density [1–3]. GaN and related compound semiconductors have generated significant interest as regards use in optoelectronic device applications due to the material's large direct band gap [4]. These epilayers exhibit a multiplicity of structural defects such as threading and misfit dislocations, nanopipes, and inversion and translation domain boundaries (IDBs and TDBs) [5, 6]. For the development of a defect model of nitride epilayers it is necessary to consider all admissible defects and defect interactions in correlation with experimental observations.

TDBs have been shown to form on $\{1\bar{2}10\}$ planes and have also been termed stacking mismatch boundaries, or prismatic stacking faults (SFs) [7, 8]. Their formation has been attributed to the coexistence of particular interfacial structures at the epitaxial interface, as well as to the Secco d'Aragona and Delavignette [9] coalescence mechanism [7, 8, 10–12]. In the present work we concentrate on 'disconnections' of TDB structure. The term 'disconnection' has been introduced by Hirth [13] to define the generic linear interfacial discontinuity with

[3] Author to whom any correspondence should be addressed.

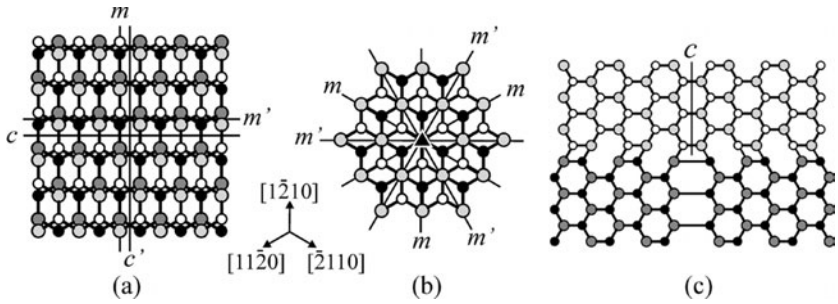

Figure 1. (a) Schematic illustration of dichromatic complex for D-TDB. Projections of symmetry and antisymmetry elements are indicated. (b) Dichromatic complex for the A-TDB. (c) Dislocation due to suppressed symmetry in A-TDB. The projection of the interrelating c-glide–mirror plane is indicated ([0001] projection. Circle size indicates distinct atomic species; white and black denote components λ and μ respectively; shading denotes atoms at height $-c/8$.)

combined dislocation and step character, and it is employed here extended to include also the facet junction morphological feature. A rigorous methodology for the study of disconnections has been developed by Hirth and Pond [14], in relation to their role in accommodating structure and phase transformations. In section 2, an account of TDB disconnections is given and the results are discussed in relation to experimental observations in section 4.

2. Admissible disconnections

Two principal structural models have been observed for $\{1\bar{2}10\}$ TDBs in GaN [8, 11, 12]; one model was proposed by Drum [15] while the other was given by Amelinckx and co-workers [16]. The former, designated henceforth as D-TDB, exhibits a relative displacement $\boldsymbol{p} = (1/2)[10\bar{1}1]$, while the latter, designated A-TDB, introduces a displacement equal to $(1/6)[20\bar{2}3]$, assuming a $(1\bar{2}10)$ boundary. In the present section we determine TDB disconnections using bicrystallography [17] under the mathematical framework of [18] as described in [14].

Hexagonal GaN crystallizes in the wurtzite structure ($P6_3mc$) which does not exhibit the highest order of symmetry for the hexagonal system, and hence can be considered a daughter structure of a parent with space group $P6_3/mmc$ [21]. Let us consider a $(1\bar{2}10)$ TDB and distinguish the crystal components on either side of the TDB by designating them as white (λ) and black (μ). We then imagine the parent structures of λ and μ to interpenetrate, thus leading to the formation of a dichromatic pattern [17] with space group $P6_3/mmc1'$ (notice that antisymmetry is employed to describe operations that interrelate the two components—see [17] for details). In a second stage, a dichromatic complex [17] is formed by taking the actual λ and μ components to interpenetrate and imposing the TDB translation between them. Figures 1(a) and (b) illustrate dichromatic complexes for the D-TDB ($P2_1mc1'$) and the A-TDB ($P6'mm'$) respectively.

The above dissymmetrization procedure yields the suppressed symmetry on account of a TDB, and we consider its implications below, starting with the A-TDB. The coset analysis [18] of $P6_3/mmc1'$ with respect to $P6'mm'$ shows that there are four complex variants that are interrelated by the operations $c_{(10\bar{1}0)}$ (the $(10\bar{1}0)$ glide–mirror), $\bar{1}$ (the inversion), and $2_{[10\bar{1}0]}$ (the 180° rotation along $[10\bar{1}0]$). Figure 1(c) illustrates the coexistence of two variants interrelated by $c_{(10\bar{1}0)}$. It is seen that a dislocation delineates their coexistence; its Burgers vector is obtained

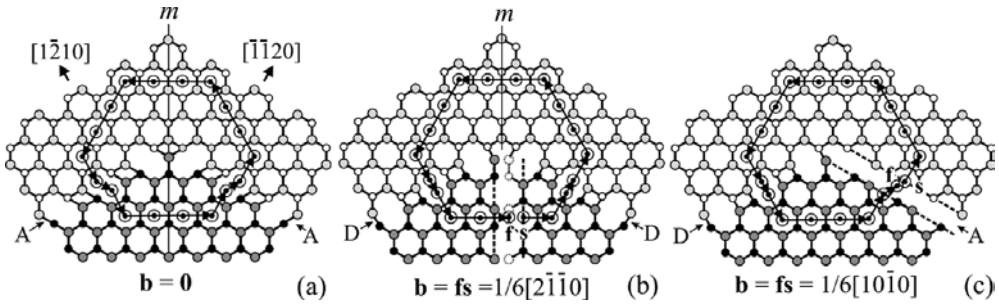

Figure 2. (a) Schematic illustration of 120° facet junctions between (a) A-TDB variants, (b) D-TDB variants, and (c) an A-TDB and a D-TDB. Circuits for defect characterization are shown and, in (a) and (b), the projection of the interrelating mirror operation has been indicated. Parts (b) and (c) are Volterra-like diagrams [14, 19] of junctions with dislocation character. The surfaces that are created by the Volterra cut are indicated by dashed lines; the dislocations are introduced by elastic deformation so as to accommodate the closure failures $\boldsymbol{fs}$ (= $\boldsymbol{b}$). The line direction of the dislocations is normal to the plane of the paper pointing outwards, in agreement with the rh/fs convention [14, 19]. (The projection and symbols are as for figure 1.)

a priori from the equation [14]

$$\mathcal{Q}_{ij} = \mathcal{W}(\lambda)_j \mathcal{P} \mathcal{W}(\mu)_i^{-1} \mathcal{P}^{-1} \tag{1}$$

where $\mathcal{W}(\lambda)_j = W(\mu)_i = (\mathrm{M}_{(10\bar{1}0)}, \boldsymbol{c}/2)$ is the glide–mirror operator in Seitz notation [18] ($\mathrm{M}_{(10\bar{1}0)}$ and $\boldsymbol{c}/2$ are the orthogonal and translation parts respectively), and $\mathcal{P} = (\mathrm{I}, \boldsymbol{p})$ where I is the identity and $\boldsymbol{p}$ is the relative displacement of μ with respect to λ. By substitution, equation (1) yields $\mathcal{Q}_{ij} = (\mathrm{I}, \boldsymbol{b}_{ij})$ where $\boldsymbol{b}_{ij} = (1/3)[10\bar{1}0]$ is the Burgers vector. The dislocation does not have an associated morphological character, given that the glide–mirror conserves the orientation of the TDB (since $\mathrm{M}_{(10\bar{1}0)} \cdot \boldsymbol{n} = \boldsymbol{n}$ where $\boldsymbol{n}$ is the unit normal to the boundary) as well as the location of its plane (since $\boldsymbol{n} \cdot \boldsymbol{c}/2 = 0$).

In a similar manner, we may employ the inversion operation in order to describe the interaction of an IDB with an A-TDB, and the operation $2_{[10\bar{1}0]}$ describes the more complex interaction of an IDB and a TDB plus the dislocation of figure 1(c).

We have indicated for the A-TDB that a dislocation may appear without change in TDB orientation. On the other hand, if we consider the TDB to facet to crystallographically equivalent orientation at 120°, as depicted in figure 2(a), the facet junction line does not exhibit dislocation character since the symmetry operations that interrelate these variants (such as the ($\bar{2}$110) mirror indicated in figure 2(a)) belong to the dichromatic complex space group $P6'mm'$.

A similar analysis may be undertaken for the D-TDB. It is found that dislocations such as those described for the A-TDB are not admissible since the aforementioned suppressed symmetry operations are conserved in this case. Conversely, 120° junction lines will exhibit stair-rod dislocation character since the interrelating operations are suppressed in the dichromatic complex. Figure 2(b) illustrates such a disconnection with a Volterra-like diagram [14, 19]. The Burgers vector is obtained from equation (1) by employing $\boldsymbol{p} = (1/2)[10\bar{1}1]$ and the ($\bar{2}$110) mirror operator; this yields $\boldsymbol{b}_{ij} = (1/6)[2\bar{1}\bar{1}0]$.

In our discussion so far we have considered disconnections between crystallographically equivalent and hence energetically degenerate regions of TDB structure. To these we may add the lattice dislocations which are admissible for residing on TDBs, as has been observed [20]. Another class of disconnections are those that accommodate the coexistence of distinct TDB structures. For example, a dislocation with Burgers vector equal to $(1/6)[10\bar{1}0]$ will accommodate a transformation from the A-TDB to the D-TDB or vice versa. Figure 2(c) is

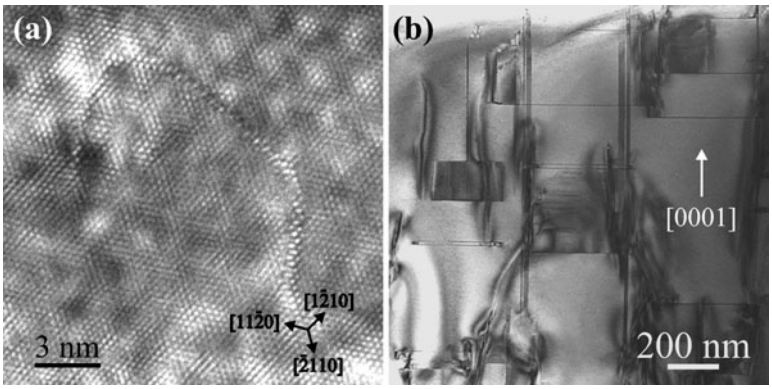

Figure 3. (a) Plan-view HRTEM micrograph illustrating a faceted TDB in the AlN buffer. Moiré fringes are visible due to the overlapping with the substrate. (b) An XTEM micrograph illustrating basal SFs interconnected with TDBs on prismatic planes.

a Volterra-like diagram of another disconnection: a 120° junction accommodating a D-to-A-TDB transformation with Burgers vector $(1/6)[10\bar{1}0]$. The defects of figures 2(b) and (c) are also in agreement with the requirement for nodal continuity with the stair-rods that delineate the 90° junctions of I_1 SFs with D-TDBs [8, 12].

3. Experiment

Specimens were obtained from GaN epilayers deposited on (0001) Al_2O_3 by RF plasma molecular beam epitaxy (MBE). Prior to deposition, the sapphire surface had undergone high-T nitridation, followed by low-T deposition of a 8–20 nm AlN buffer layer. Samples were prepared for plan-view (PVTEM) observation along $[000\bar{1}]$ and XTEM along $\langle\bar{1}2\bar{1}0\rangle$. HRTEM observations were performed using a Topcon 002B microscope, operating at 200 kV, with a point resolution of 0.18 nm and $C_s = 0.4$ mm. Image simulations for the identification of TDB structure on HRTEM micrographs were performed using the multislice algorithm in the EMS software [21]. Supercells were created in $\langle 0001\rangle$ projection for each TDB structural model. In order to establish the working conditions, a through-focus versus thickness map of perfect GaN was calculated.

4. Results and discussion

TDBs were observed at different thickness levels indicating that the epitaxial as well as the coalescence mechanisms are active for TDB introduction. Figure 3(a) is a PVTEM micrograph illustrating a TDB in the AlN buffer. Figure 3(b) is an XTEM micrograph illustrating basal SFs interconnected through TDBs in agreement with [9].

In many instances the TDBs exhibited faceting at equivalent orientations subtending a 120° angle. Figure 4(a) illustrates a 120° junction that comprises one D-TDB and one A-TDB. Using the tunnels in the structure (or equivalently the inversion centres of the parent structure of GaN—see [22]), a closed Burgers circuit has been indicated around the junction, in order to determine its character. Circuit mapping identifies this junction as a disconnection of the type depicted in figure 2(c) where a similar circuit of smaller dimensions has been mapped and closure failure $\boldsymbol{fs}$ arises. Figure 4(b) illustrates an adjacent 120° junction that comprises two A-TDBs. Again a closed circuit has been indicated, and circuit mapping identifies this junction to be of the type shown in figure 2(a) (where a similar circuit has also been indicated).

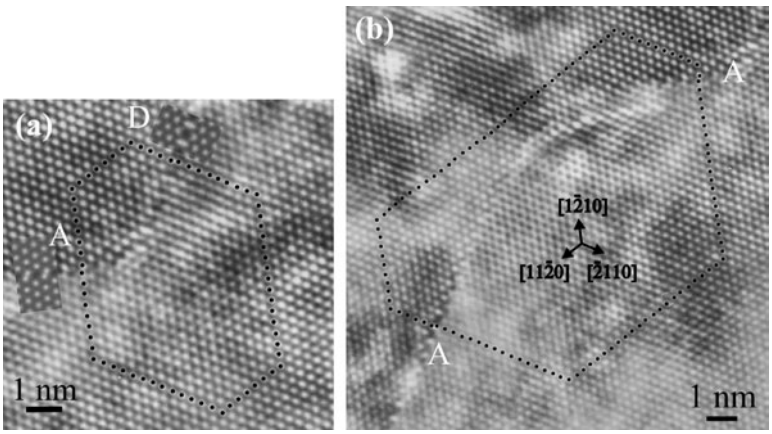

Figure 4. Plan-view HRTEM micrographs illustrating 120° TDB disconnections between (a) a D-TDB and an A-TDB, and (b) two A-TDBs. Closed circuits, indicated around the junctions, were introduced in order to identify their defect character. The circuits are placed at sufficient distances from the junction lines to avoid local bendings of planes that create contrast variations. In (a), image simulations are given as insets (thickness = 7.8 nm, defocus = −19 nm; bright spots correspond to atomic columns).

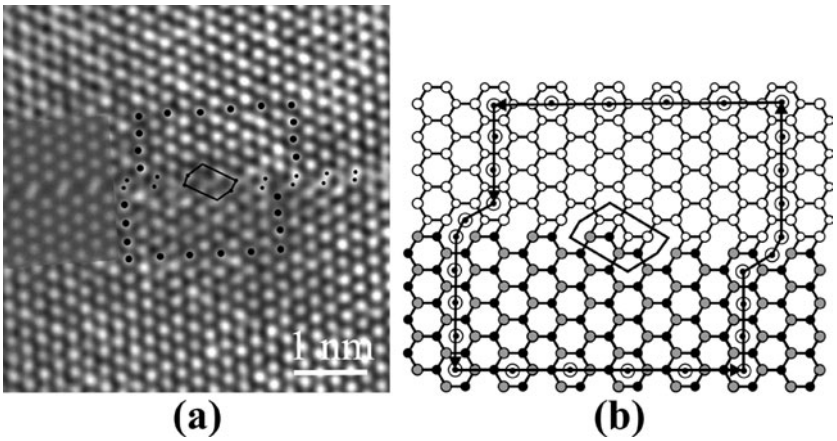

Figure 5. (a) Plan-view HRTEM micrograph of a dislocation-free step in an A-TDB. A closed circuit is indicated to characterize the step character. An image simulation is shown as an inset (thickness = 9.1 nm, defocus = −29 nm; bright spots are atomic columns). (b) Mapping of the circuit of (a) to the reference space; no closure failure arises. (The projection and symbols are as for figure 1.)

A 120° disconnection of the type depicted in figure 2(b) has been presented by Kret *et al* [20]. In addition to 120° junctions, TDBs were observed to contain dislocation-free steps as depicted in figure 5 where circuit mapping shows that no closure failure arises.

Figure 6(a) illustrates a disconnection through which an A-TDB coexists with a segment of D-TDB that is terminated by a partial dislocation. Circuit mapping is again employed to show that the disconnection between the A-TDB and D-TDB exhibits combined dislocation and step character. The step has a height of three interplanar spacings, whereas the dislocation has $\boldsymbol{b} = (1/6)[10\bar{1}0]$. Due to the particular step, the core of the dislocation is rather spread. The circuit is shown mapped to the reference space in figure 6(b).

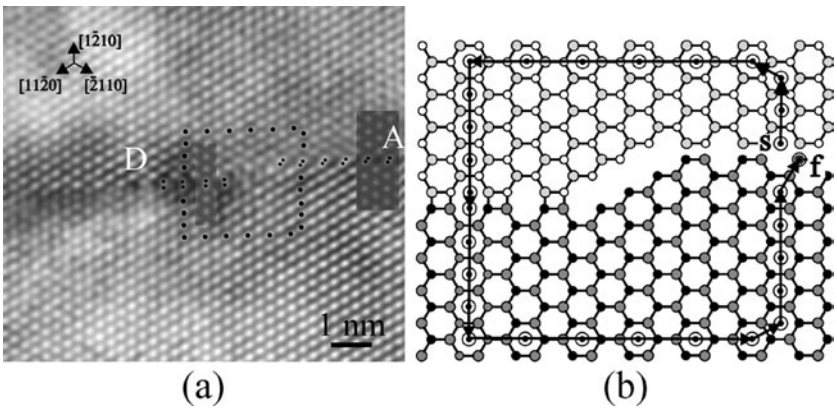

Figure 6. (a) Plan-view HRTEM micrograph of a disconnection accommodating the coexistence of an A-TDB and a D-TDB segment. A closed circuit has been introduced to characterize the disconnection. Image simulations are shown as insets (thickness 7.8 nm, defocus $= -19$ nm; bright spots are atomic columns). (b) Mapping of the circuit of (a) to the reference space. Closure failure $\boldsymbol{fs}$ appears (the projection and symbols are as for figure 1).

In discussing our results we point out that A-TDBs were frequent in our specimens despite calculations showing these boundaries to be less energetically favourable with respect to the D-TDB [12, 23]. A-TDBs can be stable if they are bounded between I_1 SFs that are a few nanometres apart [12]. In addition, A-TDBs may be stabilized at 120° junctions since the disconnection of figure 2(c) exhibits a Burgers vector of smaller magnitude than that of figure 2(b). A-TDBs may then adopt energetically degenerate orientations without the requirement for a dislocation, as shown in figures 2(a) and 4(b).

5. Conclusions

An *a priori* analysis has led to the determination of admissible disconnections in $\{1\bar{2}10\}$ TDBs in hexagonal GaN. Such features have been observed experimentally by HRTEM. Disconnections accommodate the coexistence of variants, as well as transformations between the two principal TDB structural models, and may lead to the stabilization of the high-energy TDB model.

Acknowledgment

This paper was supported by EU contract No HPRN-CT-1999-00040.

References

[1] Pankove J I and Moustakas Th D (ed) 1998 *Gallium Nitride (GaN) I (Semiconductors and Semimetals vol 50)* (New York: Academic)
[2] Ponce F 2000 *Introduction to Nitride Semiconductor Blue Lasers and Light Emitting Diodes* ed S Nakamura and S F Chichibu (London: Taylor and Francis) p 105
[3] Lahreche H, Vennegues P, Beaumont B and Gibart P 1999 *J. Cryst. Growth* **205** 245
[4] Nakamura S 1998 *Science* **281** 956
[5] Kehagias Th, Komninou Ph, Nouet G, Ruterana P and Karakostas Th 2001 *Phys. Rev.* B **64** 195329
[6] Dimitrakopulos G P, Komninou Ph, Kioseoglou J, Kehagias Th, Sarigiannidou E, Georgakilas A, Nouet G and Karakostas Th 2001 *Phys. Rev.* B **64** 245325

[7] Sverdlov B N, Martin G A, Morkoç and Smith D J 1995 *Appl. Phys. Lett.* **67** 2063
[8] Xin Y, Brown P D, Humphreys C J, Cheng T S and Foxon C T 1997 *Appl. Phys. Lett.* **70** 1308
[9] Secco d'Aragona F and Delavignette P 1966 *J. Physique Coll.* **27** C3 121
[10] Pirouz P 1998 *Mater. Sci. Forum* **264–268** 399
[11] Vermaut P, Ruterana P, Nouet G and Morkoç H 1997 *Phil. Mag.* A **75** 239
[12] Ruterana P and Nouet G 2001 *Phys. Status Solidi* b **227** 177
[13] Hirth J P 1994 *J. Phys.: Condens. Matter* **55** 985
[14] Hirth J P and Pond R C 1996 *Acta Mater.* **44** 124749
[15] Drum C M 1965 *Phil. Mag.* **11** 313
[16] Blank H, Delavignette P, Gevers R and Amelinckx S 1964 *Phys. Status Solidi* **7** 747
[17] Pond R C and Vlachavas D S 1983 *Proc. R. Soc.* A **386** 95
[18] Hahn T (ed) 1983 *International Tables for Crystallography* (Dordrecht: Reidel)
[19] Hirth J P and Lothe J 1992 *Theory of Dislocations* (Malabar, FL: Krieger)
[20] Kret S, Ruterana P and Nouet G 2000 *J. Phys.: Condens. Matter* **12** 10249
[21] Stadelmann P A 1987 *Ultramicroscopy* **21** 131
[22] Dimitrakopulos G P, Komninou Ph and Pond R C 2001 *Phys. Status Solidi* b **227** 45
[23] Northrup J E 1999 *Physica* B **273–274** 130